Available online at www.sciencedirect.com
SCIENCE DIRECT
Tectonophysics 416 (2006) 101–112
TECTONOPHYSICS
www.elsevier.com/locate/tecto

The state of the upper mantle beneath southern Africa

Keith Priestley [a,*], Dan McKenzie [a], Eric Debayle [b]

[a] Department of Earth Sciences, Bullard Laboratories, University of Cambridge, Cambridge CB3 0EZ, UK
[b] Ecole et Observatoire des Sciences de la Terre, Université Louis Pasteur, Strasbourg, France

Accepted 28 November 2005
Available online 17 February 2006

Abstract

We present a new upper mantle seismic model for southern Africa based on the fitting of a large (3622 waveforms) multi-mode surface wave data set with propagation paths significantly shorter ($\leq$6000 km) than those in globally-derived surface wave models. The seismic lithosphere beneath the cratonic region of southern Africa in this model is about 175±25 km thick, consistent with other recent surface wave models, but significantly thinner than indicated by teleseismic body-wave tomography. We determine the in situ geotherm from kimberlite nodules from beneath the same region and find the thermal lithosphere model that best fits the nodule data has a mechanical boundary layer thickness of 186 km and a thermal lithosphere thickness of 204 km, in very good agreement with the seismic measurement. The shear wave velocity determined from analyzes of the kimberlite nodule compositions agree with the seismic shear wave velocity to a depth of ~150 km. However, the shear wave velocity decrease at the base of the lid seen in the seismic model does not correspond to a change in mineralogy. Recent experimental studies of the shear wave velocity in olivine as a function of temperature and period of oscillation demonstrate that this wave speed decrease can result from grain boundary relaxation at high temperatures at the period of seismic waves. This decrease in velocity occurs where the mantle temperature is close to the melting temperature (within ~100 °C).

Keywords: Southern Africa; Surface waves; Kimberlite nodules; Upper mantle; Lithosphere

1. Introduction

Archean and Proterozoic shields form the oldest parts of the crust and lithosphere and are therefore of particular importance in understanding the early evolution of the Earth and the stabilization of the continents. They are also the only regions where we have samples of mantle material from depths greater than about 70 km whose physical properties can be measured directly and compared with in situ velocities determined from seismic studies. These samples come from kimberlite eruptions that bring mantle nodules to the surface. Because the lithosphere beneath the shields is thick and the magmas that transport the nodules to the surface are generated at the base of the lithosphere, kimberlites bring up nodules from greater depths than do alkali basalts that constitute the typical magma-type of eruptions found throughout the younger parts of continents. Since these nodules contain garnet, clinopyroxene and orthopyroxene, the pressures and temperatures at which they last equilibrate can be estimated from their mineral compositions.

The depth extent of the continents has been in question for over four decades (MacDonald, 1963). Jordan (1975) proposed that the oldest parts of the

* Corresponding author.
E-mail address: keith@esc.cam.ac.uk (K. Priestley).

0040-1951/$ - see front matter © 2006 Elsevier B.V. All rights reserved.
doi:10.1016/j.tecto.2005.11.024

continents – the shields – are underlain by a layer about 400 km thick composed of high-velocity, low density material which he termed the "tectosphere." Since the shields must carry these high velocity roots with them as the continents drift, the question of the depth extent of the continents is also of major geodynamic significance. The first seismic tomography models which were derived from body waves and long-period surface wave data supported the tectosphere model with high-velocity continental roots extending to over 400 km depth (e.g. Woodhouse and Dziewonski, 1984; Montagner and Tantimoto, 1991). However, more recent work which includes both long and short period surface wave data (e.g. Debayle and Kennett, 2000a; Priestley and Debayle, 2003; Ritsema et al., 2004) shows the high velocity roots beneath the oldest parts of the continents extend no deeper than ~200 km, in agreement with the petrological estimates (e.g. Boyd et al., 1985) which do not support cratonic roots extending deeper than ~200 km.

The Kalahari craton (Ashwal and Burke, 1989) of Southern Africa, consisting of the Kaapvaal and Zimbabwe cratons, the Limpopo mobile belt, and the Namaqua Belt (Fig. 1), has formed a stable unit for the past 2.3 Ga (McElhinny and McWilliams, 1977). In the discussion below, we are principally concerned with the Kalahari craton because its seismic structure has been recently intensively studied and because a great deal of petrological and geochemical work has been carried out on the mantle nodules from the kimberlite pipes of southern Africa. Qiu et al. (1996) used both multi-mode high frequency surface wave data whose propagation paths were largely confined to the Kalahari craton and petrologic data from kimberlite pipes on the Kalahari craton, to show that a relatively thin, high-velocity lid exists in the upper mantle beneath southern Africa with lower shear wave velocities at deeper depths in the upper mantle. Priestley (1999) and Priestley and McKenzie (2002) found from a re-examination of the data studied by Qiu et al. (1996) and the analysis of additional data, that the seismic lithosphere, which we equate to the high velocity upper mantle lid, beneath southern Africa extended at least to a depth of ~160 km. Ritsema and van Heijst (2000) used 40–200 s

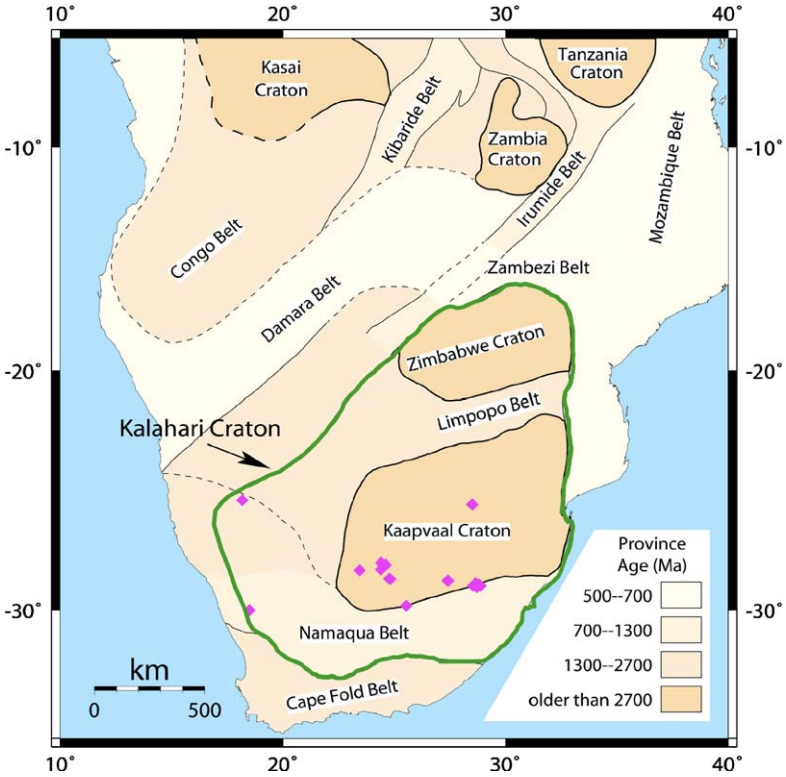

Fig. 1. Tectonic map of southern Africa. Most of southern Africa consists of Archean blocks and intervening mobile belts. The Kalahari craton (Ashwal and Burke, 1989) is composed of the Kaapvaal and Zimbabwe cratons, the Limpopo mobile belt and the Namaqua Belt. The Kalahari craton has been a stable unit for the past 2.3 Ga (McElhinny and McWilliams, 1977). Diamonds denote the locations of the kimberlite pipes of southern Africa.

fundamental mode surface waves and found that the high velocity mantle lid beneath southern Africa extends to 180–200 km. On the other hand, the recent body wave studies of Zhao et al. (1999) and James et al. (2001) find the high velocity upper mantle beneath southern Africa extends to 300–400 km depth. Hence, there is still no consensus on the state of the upper mantle beneath southern Africa. In this paper, we use the densest surface wave data set yet assembled for southern Africa to elucidate the three-dimensional (3D) upper mantle velocity structure beneath the Kalahari craton and compare the seismic results with velocities estimated from the southern African kimberlite nodules.

2. Seismic constraints on the upper mantle beneath southern Africa

We construct the 3D upper mantle model for southern Africa employing the two-step procedure previously used for Australia (Debayle and Kennett, 2000b), eastern Africa (Debayle et al., 2001) and Siberia (Priestley and Debayle, 2003). We first use the automated version (Debayle, 1999) of the Cara and Lévêque (1987) waveform inversion technique to determine a one-dimensional (1D) path average upper mantle velocity model compatible with an observed surface wave seismogram. We then combine the 1D velocity models in a tomographic inversion using the continuous regionalization algorithm of Montagner (1986) as modified by Debayle and Sambridge (2004) to obtain at each depth (50 to 400 km in steps of 25 km) the local *Sv*-wave speed (see Debayle and Kennett (2000a) for details). We directly extract from the surface waves the velocity and azimuthal anisotropy structure as a function of depth. This gives a much clearer indication of the properties at depth than do group and phase velocity maps which represent a weighted average of the earth structure over a frequency-dependent depth interval.

The analysis method we employ is based on two assumptions: that the observed surface waveform can be represented by multi-mode surface waves propagating (1) independently along the (2) great circle path between the earthquake and seismograph. These assumptions are valid for a smoothly varying medium without strong lateral velocity gradients (Woodhouse, 1974). Kennett (1995) examined the validity of the great circle approximation for surface wave propagation at regional continental scale and concluded that it was valid at longer periods (>50 s) where surface waves cross major structural boundaries, such as the continent–ocean transition. Significant derivations from great-circle propagation have been observed for shorter period (<40 s) surface waves (Alsina et al., 1993; Cotte et al., 2000), but surface wave ray tracing in earth models (Yoshizawa and Kennett, 2002) similar to the one presented here confirms that off-great circle propagation can reasonably be neglected for the fundamental and first few higher modes at periods greater than ~40s and for paths less than ~10,000 km. Ritzwoller et al. (2002) examined the effects of off-great circle propagation and found that for short path lengths (~5000 km) such as those primarily used in this study, the great circle assumption was adequate but led to increasing bias in the inverted model as path length increased. Sieminski et al. (2004) show that using a dense path coverage of relatively short paths and assuming ray theory, it is possible to detect heterogeneity with length scales smaller than the wavelength of the data set. We therefore have restricted our analysis to relatively short paths (≤6000 km) compared to those used in global studies.

Marquering et al. (1996) examined the effect of mode coupling. Body waves can be synthesized by summing large numbers of short period higher mode surface waves, but the way in which body waves and surface waves sample the structure is different: surface waves are sensitive to the average structure along the propagation path while body waves are most sensitive to the velocity structure near the geometrical ray turning point. This difference is resolved when mode coupling is taken into account. In synthetic experiments, Marquering et al. (1996) found that when they summed a large number of higher modes and neglected mode-coupling, the shallow parts of the inversion model which are sampled by the fundamental mode and the first few higher modes were reasonably accurate, but the deeper parts (~400 km) of the inversion model could differ significantly from the true model. To minimize artifacts in our model due to neglecting mode coupling, we restrict our analysis to the fundamental and first four higher Rayleigh modes in the 50–160 s period band. Sensitivity kernels (Debayle et al., 2001) show that using the fundamental and up to the fourth higher mode in this period range achieves good sensitivity over the whole upper mantle.

Kennett (1995) also demonstrated that the source contribution is not confined to the immediate neighborhood of the epicenter and the source excitation computation is improved by using a structure specific to the source region. In computing the source excitation, we take the source region velocity structure from the 3D model 3SMAC (Nataf and Ricard, 1996) and analyze the seismograms using a modified (smoothed) version of PREM (Dziewonski and Anderson, 1981) for the upper mantle velocity structure (see Fig. 3e below) both for the reference model used in

extracting the modal information from the seismogram and for the starting inversion velocity model used in determining the path-average mantle structure. However, each path has a path-specific crustal model determined by averaging the crustal part of 3SMAC along the path. Cara and Lévêque (1987) show that for their technique, the final velocity structure is weakly dependent on the reference model. In addition, at 50 s period the maximum sensitivity of even the fundamental mode is located below the crust, so that our dataset is primarily sensitive to upper mantle structure. Therefore, we assume the crustal structure is known and invert for the upper mantle structure. However, errors in the assumed crustal structure will influence the shallow mantle structure. The structure of the southern Africa crust is relatively well known (Nguuri et al., 2001). Where the crust is of similar thickness to that of southern Africa but variations are less well known, Debayle and Kennett (2000a) show that reasonable errors in crustal thickness have little effect on the mantle structure below 100–125 km depth.

Fig. 2 shows the data used in building our 3D seismic model. Fig. 2a shows the location of the 879 earthquakes and 199 seismographs which produced the 3622 seismograms which compose the data constraining our velocity model. A number of the seismograms were from the stations of the Kaapvaal project (James et al., 2001); hence this is the most densely sampled part of the model. Fig. 2b–c describe the path coverage in terms of Voronoi diagrams (Debayle and Sambridge, 2004). A Voronoi cell is a polygon constructed around a set of irregularly spaced reference nodes in which a "quality criterion" is achieved. Surface wave tomography is a 2D problem in which the constraint placed on the seismic structure at a given point in the model is highly dependent on the path distribution which is always irregular. The size of the Voronoi cell gives a qualitative measure of a constraint, which in our case is the smallest region where the path density and azimuthal distribution is sufficient to resolve the shear wave speed and azimuthal anisotropy (Debayle and Sambridge, 2004). Fig. 2b shows the ideal 2°×2° Voronoi cell size; Fig. 2c shows the Voronoi size we achieve for southern Africa. For all of the Kaapvaal craton and for much of the Kalahari craton we achieve the desired 2°×2° coverage.

The lateral smoothness of the 3D model is constrained by a horizontal correlation length L_{corr}. We choose L_{corr}=400 km, thus favoring a smooth model

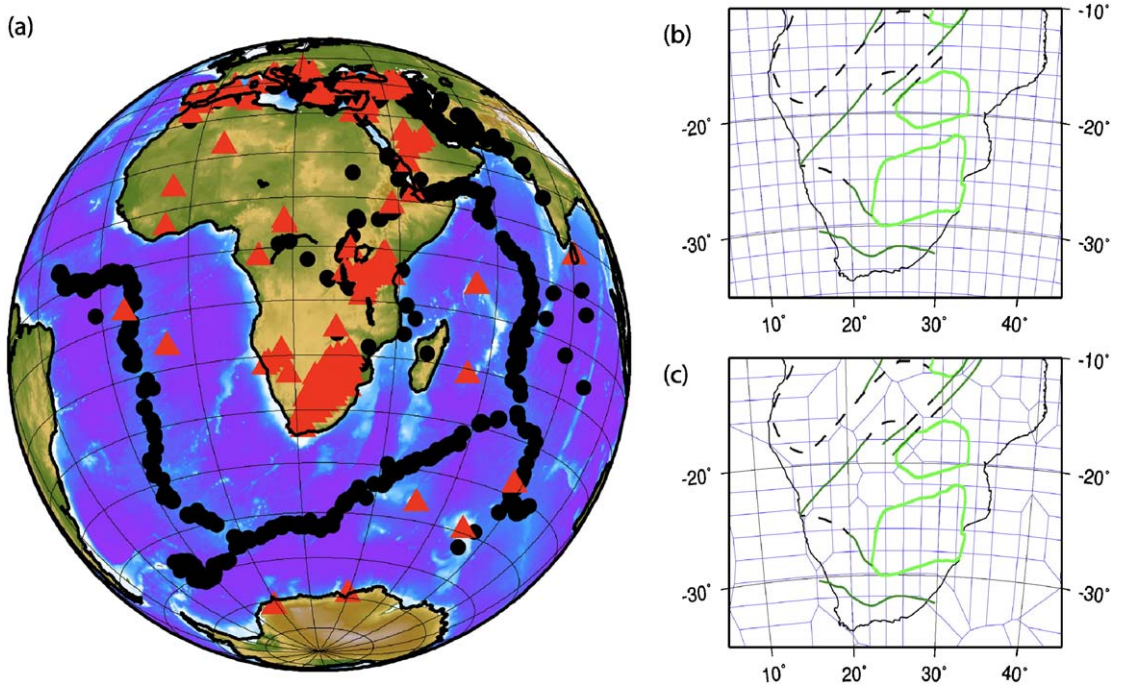

Fig. 2. Seismic data and path coverage used in building the southern Africa upper mantle model. (a) In total, we used 3622 seismograms from 879 earthquakes (black circles) recorded at 199 seismographs (red triangles). A number of the seismograms were from stations of the Kaapvaal project (large red oval in southern Africa) (James et al., 2001); hence this is the most densely sampled part of the model. (b) Idealized Voronoi diagram with 2°×2° cells and (c) achieved Voronoi diagram for the data path coverage. 2°×2° coverage is achieved for the Kaapvaal shield and most of the Kalahari craton. (For interpretation of the references to colour in this figure legend, the reader is referred to the web version of this article.)

considering our ray density and shortest wavelength used (about 200 km at 50 s period). However, although using shorter paths allows better resolution compared to global tomography, theoretical limitations resulting from the great circle approximation suggest that fine-scale structures should be interpreted cautiously (Spetzler et al., 2002).

Our seismic model for the southern Africa mantle is shown in Fig. 3. At 150 km depth (Fig. 3a) the *Sv*-wave speed is high over most of southern Africa with respect

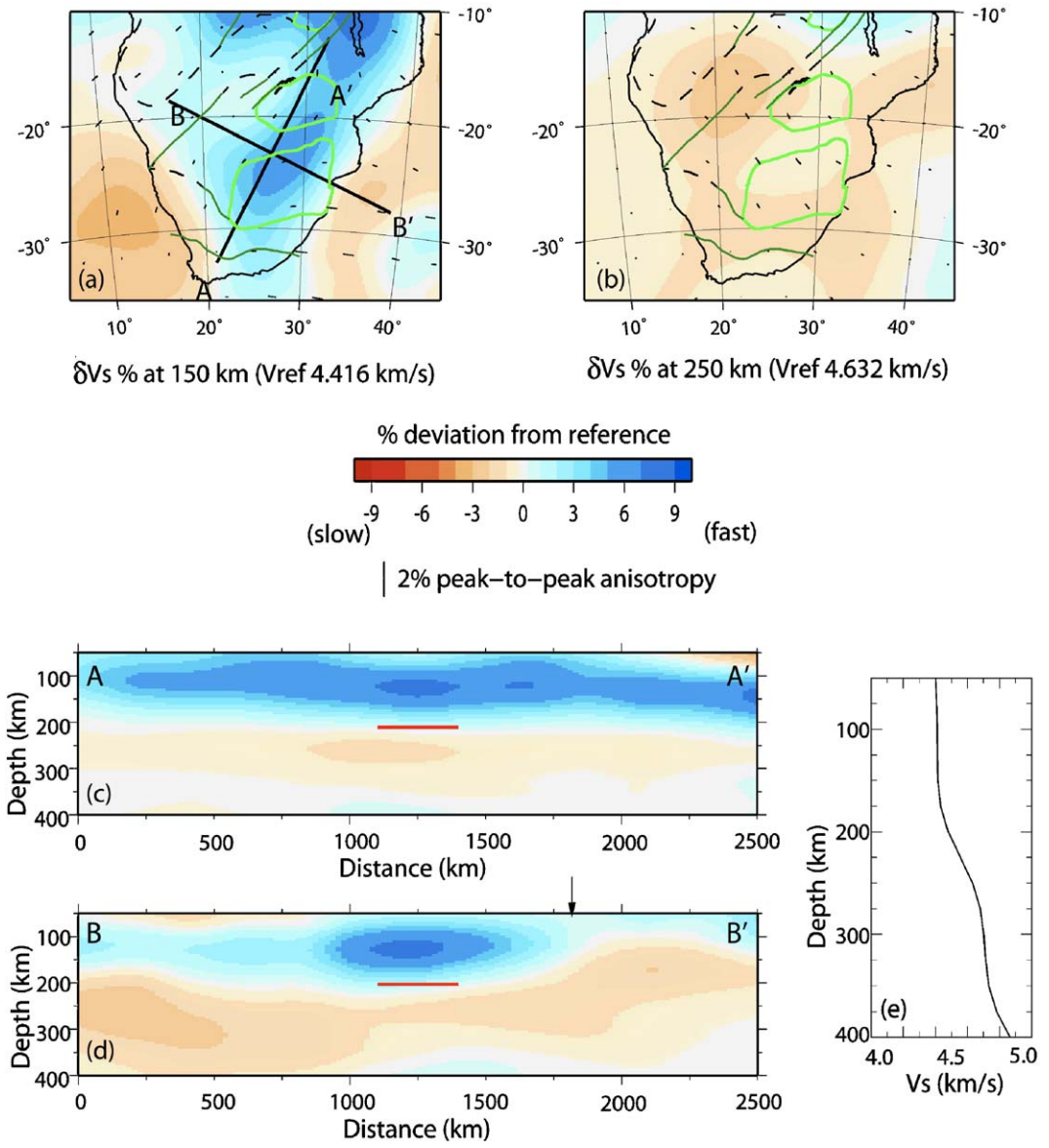

Fig. 3. *Sv*-velocity heterogeneity model for southern Africa. Depth-sections through the model are shown in (a) 150 and (b) 250 km depth. Each of the depth-sections has the velocity in the reference (V_{ref}) model at that depth indicated beneath the map. The percentage of variation from the reference velocity is denoted by the scale beneath the depth-section maps. The short black lines on the maps denote the fast direction of horizontally-propagating *Sv* waves. Two cross-sections through the model are shown in (c) and (d) and the locations of the profiles are indicated on (a). The same percentage variation scale applies to the maps and to the cross-sections. The profiles are 2500 km long and the percentage variation shown in the cross-sections is with respect to the 1D "smooth PREM" reference velocity model shown by the black solid line in (e). The vertical arrow above (d) is for reference and denotes the point at which profile BB′ intersects the coast line of SE Africa. The horizontal red lines at 204 km depth and centered at 1250 km distance on the cross-section plots (c–d) indicate the thermal lithospheric thickness measurement from the geotherm derived from the kimberlite nodule analysis shown in Fig. 5.

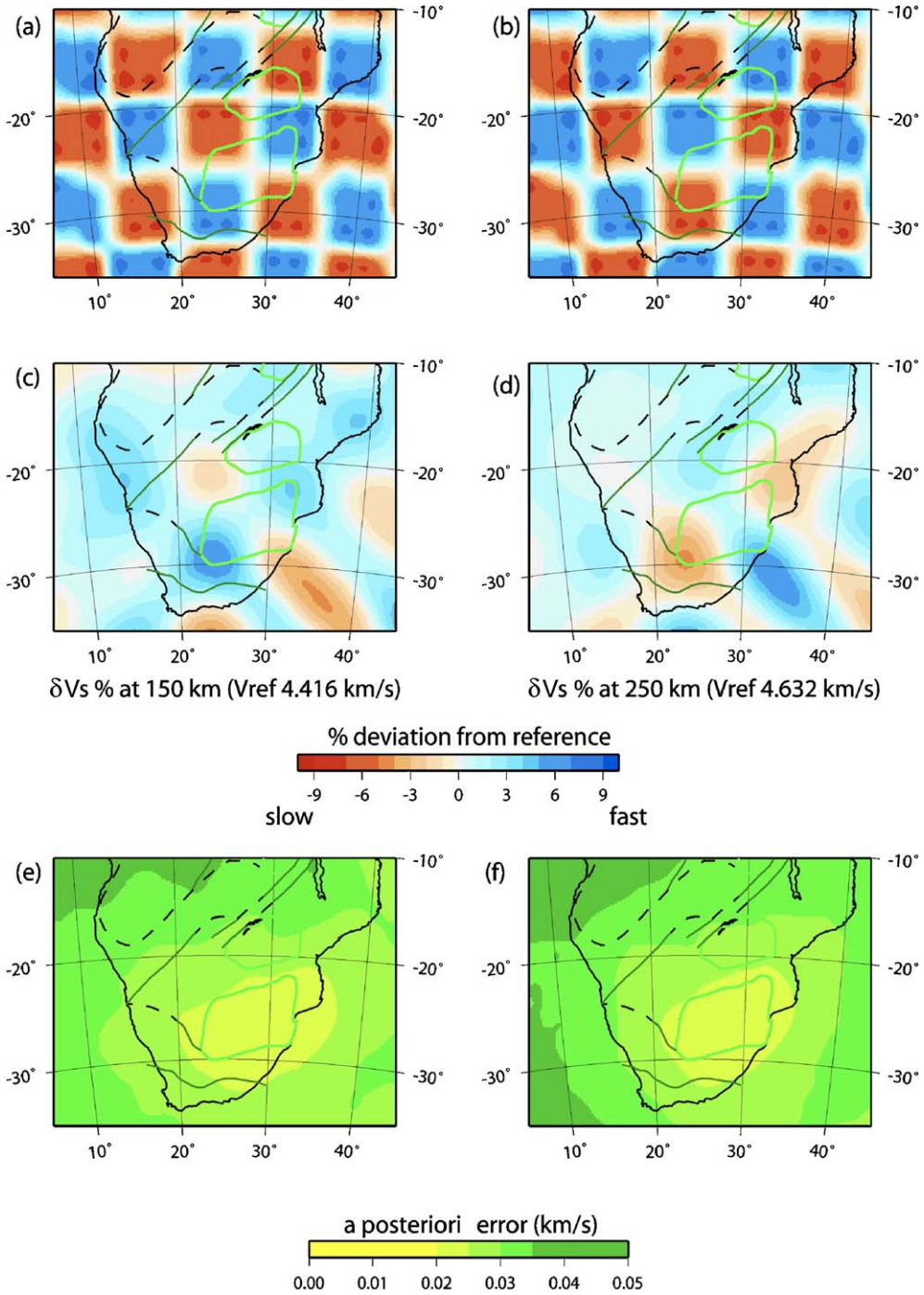

Fig. 4. Results of the checkerboard resolution test and error calculations for the seismic model. The input checkerboard models at 150 and 250 km depths are plotted in (a) and (b), respectively, and the recovered checkerboard at 150 and 250 km depths are plotted in (c) and (d), respectively. The percentage variation from the velocity at the depth in both the input and output plots is shown below the recovered model plots. Figure (e) and (f) give the a posteriori error for the model at 150 and 250 km depth. The error scale is given below the two error plots. The a posteriori error is 0.035 km/s over all of southern Africa and less than 0.025 km/s over the Kaapvaal craton.

to the reference model, and is as much as 7% high beneath then central Kalahari craton. The azimuthal anistropy at this depth is weak (~1%) beneath southern Africa. At 250 km depth (Fig. 3b) the wave speed beneath southern Africa is 1–2% below that of the reference model at this depth and there is no significant difference between the wave speed at this depth beneath the continent and the surrounding oceans. However, the Tanzania craton to the northeast of the Kalahari craton is still fast at 250 km depth with respect to the reference model. At this depth azimuthal anistropy is also small (<1%) but marginally larger in the upper mantle beneath southern Africa than in the upper mantle beneath the surrounding ocean.

Fig. 3c–d show two cross-sections through the seismic model. The profile orientations are indicated in Fig. 3a. The wave speed perturbations shown in the cross-sections are with respect to the 1D wave speed of the reference model shown in Fig. 3e. The results of the tomographic inversion are absolute *Sv*-wave speed and the direction of the fast shear wave propagation. If we plotted our results with respect to another reference model, cross-sections Fig. 3c–d would have a different visual appearance, but the information would be identical. For example, model AK135 (Kennett et al., 1995) is a "continental model" and if we used this as the reference in making Fig. 3, the relative high seen beneath the continents will be de-emphasized and the relative low beneath the oceans will be enhanced. Profile AA′ lies along the trend of the southern Africa Archean terrane and shows that high velocities with respect to the reference model extend to ~200 km depth beneath this whole region. Profile BB′ indicates that most of southern Africa is underlain by high velocity mantle to ~150 km depth with the high velocities extending to ~200 km depth beneath the Archean terrane. The arrow above Fig. 3d denotes the location of the SE African coast. There is a significant thinning of the high velocity upper mantle lid in the vicinity of the continent–ocean transition.

Fig. 4 shows the checkerboard resolution test of the seismic model. The checkerboard is made up of 7.5° square, 100 km thick blocks with a ±6% variation. The first change in velocity occurs at 125 km depth. This test shows that while there is some horizontal smearing at the edges of the model where Fig. 2c shows the Voronoi cell size increases, the recovery of the 7.5° checkboard geometry beneath southern Africa is good, but recovery of the amplitude of the anomalies decreases with depth and by ~250 km depth the amplitude is underestimated by about 50%. Fig. 4e–f show maps of the a posteriori error. It is well known that in regions where the resolution is low, the a posteriori error nearly equals the a priori error (Tarantola and Valetta, 1982). Because of the dense path coverage over southern Africa, the a posteriori error is low (<0.035 km/s) over all of this region compared to the a priori error (set at 0.05 km/s), indicating that we have good resolution over southern Africa.

3. Petrological constraints on the structure of the Kalahari craton

Upper mantle seismic velocities depend on the composition, pressure, and temperature of the rocks through which the seismic waves pass. Many kimberlites erupted through the Kalahari craton (Fig. 1) have brought up mantle nodules, and the mineralogy of such nodules can be used to estimate the pressure and temperature at which they last equilibrated, and their density and seismic velocities can then be calculated. The source of the nodule data we use is described in McKenzie (1989). We use the Finnerty and Boyd (1987) expression for the solubility of aluminum in enstatite in the presence of garnet to estimate the pressure and the Bertrand and Mercier (1985) expression for the inter-solubility of enstatite and diopside to obtain the temperature.

The steady-state temperature within the lithosphere of the Kalahari craton is calculated using the expressions in McKenzie et al. (2005). In this calculation the 35 km thick crust (Nguuri et al., 2001) is divided into two layers, both with the same thermal conductivity, 2.5 W K^{-1} m^{-1}. The heat generation rate for the upper crust is 1.12 μW m^{-3} and the lower crust is 0.4 μW m^{-3}, the values suggested by Jaupart and Mareschal (1999) for granulite. The thickness of the upper and lower crust was varied to fit the pressure and temperature estimates from the nodules while keeping the total crustal thickness equal to 35 km. The heat generation in the mantle portion of the mechanical boundary layer (MBL) is taken to be zero. At the base of the MBL the heat flux and temperature must be the same as those at the top of the thermal boundary layer (TBL). The temperature structure within the TBL was obtained from the expressions given by Richter and McKenzie (1981) and smoothly grades into the temperature of the convecting layer whose potential temperature is 1315 °C.

Fig. 5 shows the best-fitting geotherm to the nodule data, calculated using this method. The resulting thickness of the MBL is 186 km, and the base of the thermal lithosphere is at 204 km depth. The uncertainties in the mean thickness of the MBL and the thermal lithosphere beneath the Kalahari craton are probably both about 10 km. The lithosphere depth

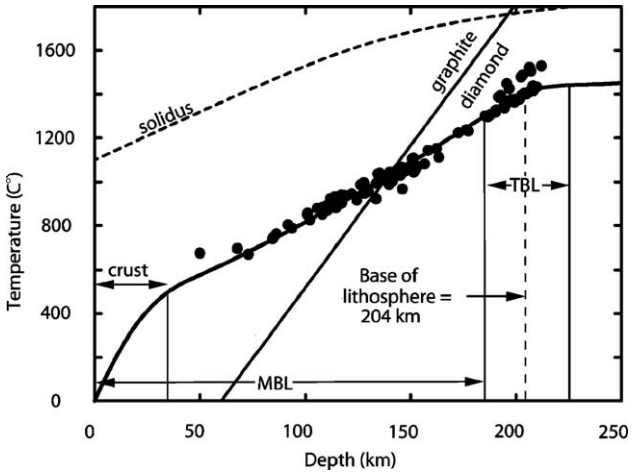

Fig. 5. Pressure and temperature estimates for nodules from the Kaapvaal craton calculated using the Finnerty and Boyd (1987) geobarometer and Bertrand and Mercier (1985) geothermometer. The solidus is from McKenzie and Bickle (1988), and the diamond-graphite phase boundary from Kennedy and Kennedy (1976). The continuous lines show the best-fitting geotherm.

determined from the nodules in Fig. 5 is also plotted in Fig. 3c–d. This shows that the transition from high velocities relative to the reference model to low velocities relative to the reference model occurs near the depth where the temperature gradient decreases sharply at the base of the thermal lithosphere.

The seismic velocities and densities can be calculated if the mineral proportions (called the modal mineralogy) have been measured in a nodule whose mineral compositions are known. Few such measurements have been made on the same nodule. Qiu et al. (1996) (see their appendix C for details) used the Tainton and McKenzie (1994) melting models to estimate the modal mineralogy, elastic parameters and density. They used four nodule suites: phlogopite K-richerite peridotite (PKP), garnet peridotite (GP) and garnet phlogopite perdotite (GPP) from Erlank et al. (1987), and the depleted and fertile nodules from Nixon et al. (1981). Qiu et al. (1996) obtained the modal mineralogy by minimizing the misfit between the bulk composition and that calculated from the mineral proportions and compositions, and then used the mineral compositions and modal mineralogy to estimate the wave speeds and density at the depths and temperatures from which the nodules came. The nodule compositions from the southern Africa vary with depth. The velocities and densities calculated from the nodules are compared with those estimated from seismology (Fig. 6). There is one important difference between the seismological and petrological velocity–depth estimates: the depth estimates from the highest pressure (deepest) nodules require them to come from within the seismically-determined low velocity zone (LVZ), yet the estimates of

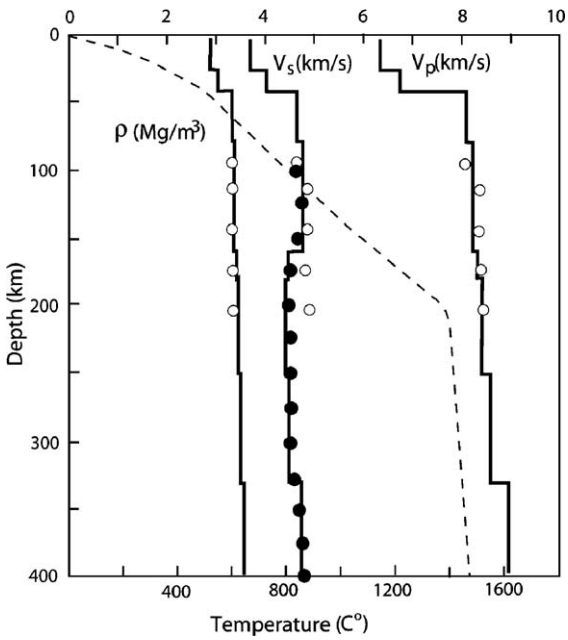

Fig. 6. Comparison of the seismic velocities and densities deduced for the Kalahari craton with velocities and densities determined from analysis of the kimberlite nodules. The thick, solid lines are the velocities and densities determined from waveform modeling three-component seismograms of southern Africa earthquakes recorded in southern Africa, whose propagation paths were largely confined to the Kalahari craton (Priestley, 1999). The solid circles are the average V_{SV} determined in this study; open circles show estimates of ρ, V_S and V_P obtained using expressions from Qiu et al. (1996) and models of nodule composition and modal mineralogy from Tainton and McKenzie (1994) for PKP nodules (92 km), depleted and GPP nodules (112 and 142 km), and fertile nodules (172 and 202 km). The dashed line is the geotherm from Fig. 5. The scale for ρ, V_S and V_P is at the top of the plot; the temperature scale is at the bottom of the plot.

V_s for nodules increase monotonically with depth (open circles). Qiu et al. (1996) and Priestley (1999) found the same discrepancy, which they suggested might be due to the presence of a small melt fraction (McKenzie, 1989) that prevented the transmission of shear stress across grain boundaries. The V_s model for southern Africa presented here (solid circles) shows a similar disparity (Fig. 6).

Important progress has occurred in our understanding of the processes that control the dependence of the shear modules on temperature and on the frequency of the seismic waves. At the temperature close to the melting point (within ~100 °C), the shear modulus depends strongly on frequency (Jackson, 2000; Gribb and Cooper, 1998). The Gribb and Cooper (1998) measurements show a decrease of more than a factor of two between periods of 3 and 100 s at a temperature of 1250 °C for the fine-grained polycrystalline sample of olivine that they used (Fig. 7). More recently, the same authors (Gribb and Cooper, 2000) have shown experimentally that this behavior does not rely upon the presence of melt. Instead, they argue that it results from transient diffusive effects that relax the stresses on subgrain boundaries (Gribb and Cooper, 1998), and that the time constant involved in this relaxation depends on d^3, where d is the size of the subgrains. The observed attenuation in the upper mantle requires a subgrain size of 35 μ (Gribb and Cooper, 1998) compared with a grain size of 3 μ used in their experiments. Their laboratory results can therefore be applied to the mantle if the periods are increased by $(35/3)^3$ (Fig. 7).

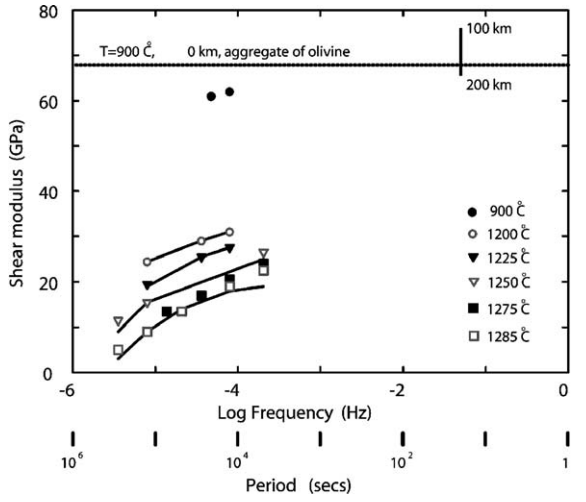

Fig. 7. The experimental points and lines are taken from Gribb and Cooper (1998), but are plotted at frequencies appropriate for a mantle grain size by dividing the experimental frequencies by $(35/3)^3$. The horizontal line shows the shear modulus of an olivine aggregate with Fo_{92} calculated at $P=0$ GPa, $T=900$ °C using the method described in the appendix of Qiu et al. (1996). The vertical line shows the shear moduli at depths of 100 and 200 km estimated from seismological observations.

Also shown in Fig. 7 is the shear modulus for an olivine aggregate which consists of 92% forsterite and 8% fayalite (Fo_{92}), and the seismological estimates at depths of 100 and 200 km, plotted at a period of 20 s. Even though none of the aggregates used by Gribb and Cooper (1998) contained melt, they show a large decrease in the shear modulus at high temperature and low frequencies. As Fig. 7 shows, the experimental results are at effective periods that are longer than those used to study the structure of the crust and mantle beneath the Kalahari craton, and so it is not yet possible to use the geotherms in Fig. 5 to calculate the seismic velocities when grain boundary relaxation occurs. But Fig. 7 clearly shows that the changes in the shear modulus caused by such relaxation are much larger than those required to account for the decrease in *Vs* between 100 and 200 km. Therefore, this decrease does not require the presence of melt.

4. Discussion and conclusions

We present a new upper mantle V_s seismic model for southern Africa based on the fitting of 3622 multi-mode surface waveform data with short propagation paths compared to those typical of global surface wave analysis. The seismic lithosphere beneath the cratonic region of southern Africa is about 175±25 km thick. Below about 200 km depth there is no significant difference in the velocity structure beneath southern Africa and the surrounding ocean. This V_{SV} model is in good agreement with V_S models for southern Africa determined from surface wave analysis of regional events with propagation paths largely confined to the Kalahari craton (Priestley, 1999). We determine the in situ geotherm from kimberlite nodules from beneath the same region and find that the lithospheric model that best fits the nodule data has a mechanical boundary layer thickness of 186 km and a thermal lithosphere thickness of 204 km, in very good agreement with the seismic measurement. The shear wave velocity decrease at the base of the lid in both the new V_{SV} model and in the V_S models determined from the regional surface wave analysis does not correspond to a change in mineralogy estimated from the kimberlite nodules from these depths. Recent experimental studies of the shear wave velocity in olivine as a function of temperature and period of oscillation (Gribb and Cooper, 1998; Jackson, 2000) demonstrate that this

wave speed decrease results from grain boundary relaxation at high temperatures at the period of seismic waves. This decrease in velocity occurs where the mantle temperature is close to the melting temperature.

Ritsema and van Heijst (2000) used fundamental mode Rayleigh wave data for periods ranging from 40 to 200 s and found V_{SV} velocities ~6% high with respect to PREM to 180–190 km depth. From 200–400 km depth, the V_{SV} velocities in their model are ~1% high with respect to PREM. At depths shallower than 200 km, our model is in good agreement with that of Ritsema and van Heijst (2000), but we do not find the weak high velocities extending to 400 km depth beneath southern Africa. This difference may arise because of the poorer resolution of the structure at depth for the fundamental modes Rayleigh waves compared to the multi-mode Rayleigh waves analyzed in this study.

Freybourger et al. (2001) determined both fundamental mode Love and Rayleigh wave phase velocities (22–100 s period) across the Kaapvaal project seismic array and find the upper mantle is radially anisotropic from beneath the Moho (5.6% anisotropy), to about 100 km depth (2.4% anisotropy). Below 100 km depth their model is isotropic and contains a weak LVZ centered at ~220 km depth and extending to 350 km depth. Qiu et al. (1996) and Priestley (1999) found no indication of the Love–Rayleigh discrepancy in their modelling of three-component, multi-mode surface waveforms (18–80 s period) for southern Africa, but found a stronger LVZ between 160 and 330 km depth, compared to that in the Freybourger et al. (2001) model. A possible explanation for the difference in the strength and depth of the LVZ in these two models is to invoke a trade-off between radial anistropy and isotropic shear wave velocity: if radial anistropy with V_{SH} faster than V_{SV} (as found by Freybourger et al., 2001) is present in the upper mantle, the isotropic shear waves velocities found by Priestley (1999) could be biased (toward intermediate values between V_{SV} and V_{SH}) at depths shallower than 100 km. The high V_{SV} velocities at depths shallower than 100 km might then be compensated by lower seismic velocities where the Love waves start to lose their resolution in the LVZ.

Such an artifact between radial anisotropy and shear wave velocity will not however, affect the inversion of Rayleigh waves alone as processed in this study, which are insensitive to radial anisotropy and should therefore provide a correct estimate of the V_{SV} velocities, providing the V_{SV} azimuthal component has been properly accounted for in the tomographic inversion. Fig. 6 shows that the average V_{SV} determined in this study based only on Rayleigh waves agrees with the isotropic shear wave velocity found by Priestley (1999) down to 400 km depth. This suggests that the LVZ found by Priestley (1999) at depths larger than 160 km does not result from an artifact related to the neglect of radial anisotropy. Gung et al. (2003) suggest that the controversy regarding the depths of the cratons comes from comparing models determined with V_{SV} data which show shallower roots with models derived from V_{SH} data which indicate deeper roots. However, as they demonstrate, this is not the case for southern Africa where upper mantle models derived from V_{SV} data have high velocity roots extending to similar or deeper depths than models derived from V_{SH} data (see their Fig. 2).

The velocity structure obtained from the analysis of near-vertical travelling body-waves data (James et al., 2001) shows higher shear wave velocities extending to 400 km depths or more beneath the Kalahari craton. However, the amplitude of the high velocity perturbation in the S-wave travel time tomography upper mantle model is ~1% with respect to an unspecified average as opposed to the 6–7% high with respect to PREM found from surface wave analysis. The apparent difference in the models derived from body wave and surface wave data arises from several factors fundamental to the analysis procedures. The body wave and surface wave analyses produce vertical and horizontal smearing, respectively, in the resulting seismic model. Horizontally travelling surface waves are more subject to horizontal smearing but provide relatively good vertical resolution in the upper mantle, whereas near-vertical travelling body-waves provide good horizontal resolution but smear the structure in the vertical dimension. The surface wave analysis provides an absolute wave speed for the seismic model. Travel-time tomographic images are determined from the inversion of relative travel-time residuals since relative arrival time can be determined more accurately than absolute arrival times. The earthquake location and origin time are redetermined in the travel-time tomography inversion to absorb the effects of earthquake location error and structure outside the Earth volume of interest. Thus, the seismic image derived from travel time tomography displays only the velocity contrast relative to the horizontal average velocity which is both unspecified and which varies with depth. Therefore, the high velocity lid and underlying LVZ seen in the seismic models for southern Africa derived from surface wave data (Fig. 3) are invisible to the travel-time tomography analysis. Because of the poor vertical resolution in the deep part of models derived from vertical travelling body waves, these models are consistent with models derived from surface waves, and with the differences resulting from

the high lid velocities being smeared over a greater depth range in the models derived from near-vertical travelling body-waves. Body wave tomography using teleseismic events can resolve lateral velocity variations, but is completely insensitive to variations in the mean vertical velocity. We therefore believe that the S-wave travel time tomography of James et al. (2001) is consistent with the horizontally averaged velocity structure shown in Fig. 3.

The best-resolved average vertical V_P and V_S structure within the high velocity lid beneath southern Africa agrees well with velocities estimated from the mineralogy of mantle nodules down to 150 km. However, the shear wave velocity decrease at the base of the lid does not correspond to a change in mineralogy. Experimental studies of the shear wave velocity in olivine as a function of temperature and period of oscillation suggest that this decrease results from grain boundary relaxation at elevated temperatures at the period of seismic waves. Since the decrease in velocity occurs where the mantle temperature is close to but below the melting temperature, such an explanation is consistent with thermal models of the temperature structure beneath the Kalahari craton. The high velocity, depleted upper mantle lid beneath southern Africa extends to an average depth of no more than about 200 km. It is underlain by material that becomes steadily less depleted with increasing depth, where the shear modulus also decreases because of the increasing temperature.

Acknowledgements

This study has benefited from discussions with M. Carra and J.J. Lévêque. DM acknowledges support of the Royal Society. This work was initiated while KP was a visiting professor at the Ecole and Observatoire des Sciences de la Terre, Université Louis Pasteur. Data for this study were obtained from the IRIS data center and uses seismograms from the GEOSCOPE, GEOFON, IRIS–IDA and IRSI–USGS permanent seismic networks and from SASEK and Tanzania PASSCAL experiments. This is Cambridge University Department of Earth Sciences contribution ES8196.

References

Alsina, D., Sneider, R., Maupin, V., 1993. A test of the great-circle approximation in the analysis of surface waves. Geophys. Res. Lett. 20 (10), 915–918.

Ashwal, L., Burke, K., 1989. African lithosphere structure, volcanism, and topography. Earth Planet. Sci. Lett. 96, 8–14.

Bertrand, P., Mercier, J.-c.C., 1985. The mutual solubility of coexisting ortho- and clinopyroxene: toward an absolute geothermometer for the natural system? Earth Planet. Sci. Lett. 76, 109–122.

Boyd, F., Gurney, J., Richardson, S., 1985. Evidence for a 150–200 km thick Archean lithosphere from diamond inclusion thermobarometry. Nature 315, 387–389.

Cara, M., Lévêque, J., 1987. Waveform inversion using secondary observables. Geophys. Res. Lett. 14, 1046–1049.

Cotte, N., Pedersen, H., Campillo, M., Farra, V., Cansi, Y., 2000. Off-great-circle propagation of intermediate period surface waves observed on a dense array in the French Alps. Geophys. J. Int. 142, 825–840.

Debayle, E., 1999. Sv-wave azimuthal anisotropy in the Australian upper mantle: preliminary results from automated Rayleigh waveform inversion. Geophys. J. Int. 137, 747–754.

Debayle, E., Kennett, B., 2000a. Anistropy in the Australasian upper mantle from Love and Rayleigh waveform inversion. Earth Planet. Sci. Lett. 184, 339–351.

Debayle, E., Kennett, B., 2000b. The Australian continental upper mantle: structure and deformation inferred from surface waves. J. Geophys. Res. 105, 25423–25450.

Debayle, E., Sambridge, M., 2004. Continuous regionalization of massive surface wave data sets: model construction and resolution assessment. J. Geophys. Res. 109. doi:10.1029/2003JB002652.

Debayle, E., Lévêque, J.-J., Cara, M., 2001. Seismic evidence for a plume in the upper mantle beneath the northeastern Afro/Arabian continent. Earth Planet. Sci. Lett. 193, 423–436.

Dziewonski, A.M., Anderson, D., 1981. Preliminary reference earth model. Phys. Earth Planet. Inter. 25, 297–356.

Erlank, A., Waters, F., Hawkesworth, C., Haggerty, S., Allsopp, H., Rickard, R., Menzies, M., 1987. Evidence for mantle metasomatism in peridotite nodules from the Kimberly Pipes, South Africa. In: Menzines, M., Hawkesworth, C. (Eds.), Mantle Metasomatism. Academic Press, London, pp. 221–311.

Finnerty, A., Boyd, F., 1987. Thermobarometry for garnet peridotites: basis for the determination of thermal and compositional structure of the upper mantle. In: Nixson, P. (Ed.), Mantle Xenoliths. Wiley and sons, New York, pp. 381–402.

Freybourger, M., Gaherty, J., Jordan, T., 2001. Structure of the Kaapvaal craton from surface waves. Geophys. Res. Lett. 28, 2489–2492.

Gribb, T., Cooper, R., 1998. Low-frequency shear attenuation in polycrystalline olivine: grain boundary diffusion and the physical significance of the Andrade model for viscoelastic rheology. J. Geophys. Res. 103, 27267–27279.

Gribb, T., Cooper, R., 2000. The effect of an equilibrated melt phase on the shear creep and attenuation behavior of polycrystalline olivine. Geophy. Res. Lett. 27, 2341–2344.

Gung, Y., Panning, M., Romanowicz, B., 2003. Global anisotropy and the thickness of continents. Nature 422, 707–711.

Jackson, I., 2000. Laboratory measurements of seismic wave dispersion and attenuation: recent progress. The Earth's Deep Interior: Mantle Physics and Tomography from the Atomic to Global Scale. Geophysical Monograph. American Geophysical Union, vol. 117. American Geophysical Union, pp. 265–289.

James, D., Fouch, M., VanDecar, J., van der Lee, S., 2001. Tectospheric structure beneath southern Africa. Geophys. Res. Lett. 28, 2485–2488.

Jaupart, C., Mareschal, J., 1999. The thermal structure and thickness of continental roots. Lithos 48, 93–114.

Jordan, T., 1975. The continental tectosphere. Rev. Geophys. 13, 1–12.
Kennedy, C., Kennedy, G., 1976. The equilibrium boundary between graphite and diamond. J. Geophys. Res. 81, 2467–2470.
Kennett, B., 1995. Approximations for surface-wave propagation in laterally varying media. Geophys. J. Int. 122, 470–478.
Kennett, B., Engdahl, E., Bulland, R., 1995. Constraints on seismic velocities in the Earth from travel times. Geophys. J. Int. 122, 108–124.
MacDonald, G., 1963. The deep structure of continents. Rev. Geophys. 1, 587–665.
Marquering, H., Sneider, R., Nolet, G., 1996. Waveform inversion and the significance of surface-wave mode coupling. Geophys. J. Int. 124, 258–278.
McElhinny, M., McWilliams, M., 1977. Precambrian geodynamics — a paleomagnetic view. Tectonophysics 40, 137–159.
McKenzie, D., 1989. Some remarks on the movement of small melt fractions in the mantle. Earth Planet. Sci. Lett. 96, 53–72.
McKenzie, D., Bickle, M., 1988. The Volume and Composition of Melt Generated by Extension of the Lithosphere, vol. 29, pp. 625–679.
McKenzie, D., Jackson, J., Priestley, K., 2005. Thermal structure of oceanic and continental lithosphere. Earth Planet. Sci. Lett. 233, 337–349.
Montagner, J., 1986. Regional three-dimensional structures using long-period surface waves. Ann. Geophys. 4, 283–294.
Montagner, J., Tantimoto, T., 1991. Global upper mantle tomography of seismic velocity and anisotropies. J. Geophys. Res. 96, 20337–20351.
Nataf, H.-C., Ricard, Y., 1996. 3SMAC: an a priori tomographic model of the upper mantle based on geophysical modelling. Phys. Earth Planet. Inter. 95, 101–122.
Nguuri, T., Gore, J., D.E.Webb, J., Wright, S., Zengeni, C., Gwavava, T., Snoke, O., Group, J., 2001. Crustal structure beneath southern Africa and its implications for the formation and evolution of the Kaapvaal and Zimbabwe cratons. Geophys. Res. Lett. 28, 2501–2504.
Nixon, P., Rogers, N., Gibson, I., Grey, A., 1981. Depleted and fertile mantle xenoliths from southern African kimberlites. Annu. Rev. Earth Planet. Sci. 9, 285–309.
Priestley, K., 1999. Velocity structure of the continental upper mantle: evidence from southern Africa. Lithos 48, 45–56.
Priestley, K., Debayle, E., 2003. Seismic evidence for a moderately thick lithosphere beneath the Siberian Platform. Geophys. Res. Lett. 30 (3). doi:10.1019/2002GL015931.
Priestley, K., McKenzie, D., 2002. The structure of the upper mantle beneath southern Africa. In: Fowler, C., Ebinger, C., Hawkesworth, C. (Eds.), The Early Earth: Physical, Chemical and Biological Development, vol. 199. Geological Society, London, pp. 45–64. Special Publications.
Qiu, X., Priestley, K., McKenzie, D., 1996. Average lithospheric structure of southern Africa. Geophys. J. Int. 127, 563–587.
Richter, F., McKenzie, D., 1981. Parameterizations for the horizontally averaged temperature of infinite Prandtl number convection. J. Geophys. Res. 86, 1738–1744.
Ritsema, J., van Heijst, H., 2000. New seismic model of the upper mantle beneath Africa. Geology 28, 63–66.
Ritsema, J., van Heijst, H., Woodhouse, J., 2004. Global transition zone tomography. J. Geophys. Res. 109. doi:10.1029/2003JB002610.
Ritzwoller, M., Shapiro, N., Barmin, M., Leshvin, A., 2002. Global surface wave diffraction tomography. J. Geophys. Res. 107 (B12). doi:10.1029/2002JB001777.
Sieminski, A., Lévêque, J., Debayle, E., 2004. Can finite-frequency effects be accounted for in ray theory surface wave tomography? Geophys. Res. Lett. 31. doi:10.1029/2004GL021402.
Spetzler, J., Trampert, J., Sneider, R., 2002. The effect of scattering in surface wave tomography. Geophys. J. Int. 149, 755–767.
Tainton, K., McKenzie, D., 1994. The generation of kimberlites, lamproites, and their source rocks. J. Petrol. 35, 787–817.
Tarantola, A., Valetta, B., 1982. Generalized nonlinear inverse problems. Rev. Geophys. 20, 219–232.
Woodhouse, J., 1974. Surface waves in a laterally varying layered structure. Geophys. J. R. Astron. Soc. 37, 461–490.
Woodhouse, J., Dziewonski, A., 1984. Three-dimensional modelling of Earth structure by inversion of seismic waveforms. J. Geophys. Res. 89, 5953–5986.
Yoshizawa, K., Kennett, B., 2002. Determination of the influence zone for surface wave paths. Geophys. J. Int. 149, 440–453.
Zhao, M., Langston, C., Nyblade, A., Owens, T., 1999. Upper mantle velocity structure beneath southern Africa from modelling regional seismic data. J. Geophys. Res. 104, 4783–4794.